



CeO₂-supported Pt/Ni catalyst for the renewable and clean H₂ production via ethanol steam reforming

Vincenzo Palma ^{a,*}, Filomena Castaldo ^a, Paolo Ciambelli ^a, Gaetano Iaquaniello ^b

^a Dipartimento di Ingegneria Industriale, Università di Salerno, Via Ponte Don Melillo 84084 Fisciano (SA), Italy

^b Tecnimont KT S.p.A., Viale Castello della Magliana 75, 00148 Roma, Italy



ARTICLE INFO

Article history:

Received 5 November 2012

Received in revised form 11 January 2013

Accepted 22 January 2013

Available online 8 February 2013

Keywords:

Hydrogen

Ethanol

Bimetallic

Steam reforming

Low temperature

ABSTRACT

The steam reforming of biomass-derived ethanol is a promising method for hydrogen production. It needs the development of efficient catalysts, especially when the reaction is carried out at temperature lower than 600 °C. The performances of a bimetallic sample, based on Pt (3 wt.%) and Ni (10 wt.%) and supported on CeO₂ were investigated, in terms of activity, selectivity and stability. Very interesting results were obtained in the range 250–600 °C, even with a stoichiometric water/ethanol molar ratio: the ethanol was completely converted at $T \geq 300$ °C, with a products distribution extremely close to the equilibrium calculations. Moreover, the selectivity towards the desired compounds was very high, and as a consequence, the sample showed a very low coke selectivity (<1%) and a high stability, that was further improved with higher amount of water in the feed stream. The analysis of the products distribution as a function of contact time (3–600 ms) and temperature (340–480 °C) and the temperature programmed desorption (TPD) experiments, were used to hypothesize the possible reactions involved, in order to develop a mathematical model, able to simulate the kinetic behaviour of the low temperature-ethanol steam reforming over Pt/Ni/CeO₂. Finally, a possible Pt/Ni/CeO₂ catalyzed reaction pathway at 370 °C, was formulated, that includes the following steps: ethanol adsorption followed by dehydrogenation to acetaldehyde; intermediate decomposition and reforming to CH₄, CO, H₂ and CO₂; CO-WGS and CO₂ methanation reaction.

© 2013 Elsevier B.V. All rights reserved.

1. Introduction

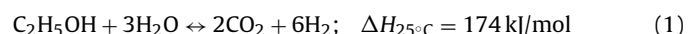
Hydrogen plays an important role as an energy carrier for the transition to the green power engineering [1,2]. It is the preferred fuel in fuel cells, and its production from methane, methanol, and gasoline has been extensively studied [3,4].

Steam reforming of natural gas is currently the dominant technology but, recently, the rising concern with the reduction of greenhouse gas emissions and atmospheric pollution increased the interest in clean and renewable feedstocks [5].

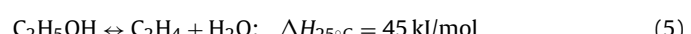
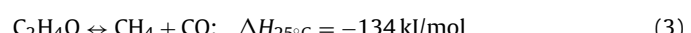
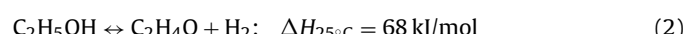
Steam reforming of ethanol (ESR) is seen as a sustainable route to feed on-line proton exchange membrane fuel cells (PEMFC) with hydrogen. This reaction is drawing much attention due to the high H₂ yield at low temperature and the non-toxic character of the reactant, which can be prepared from the renewable biomass [6,7]. It is directly usable in the ESR reaction as an aqueous solution, avoiding the costs related to the water separation processes. In addition, bio-ethanol provides a renewable carbon cycle when it is used as the feedstock for hydrogen production and the thermodynamics

properties allow high ethanol conversion at low temperature; moreover, ethanol is significantly less toxic than methanol and gasoline. Ultimately, the economic future of ethanol production looks even more favourable when one considers the likely increasing in the price of petroleum and other fossil fuels as the world's reserves are depleted [8,9].

As compared to partial oxidation (POX) and oxidative steam reforming (OSR), the ESR reaction is characterized by higher hydrogen yields, lower reaction rates and a marked endothermicity (Eq. (1))

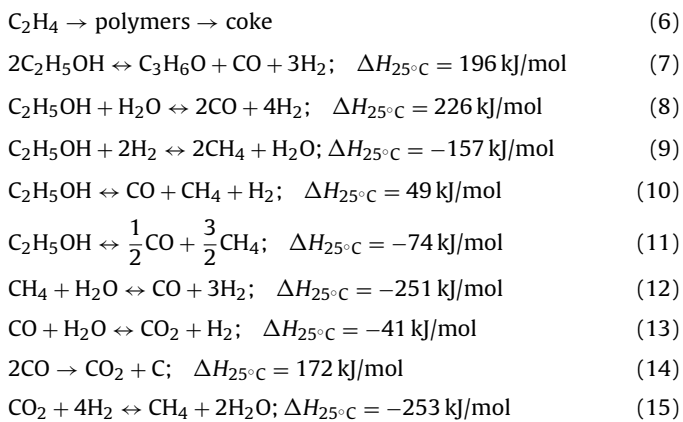


This multi-molecular reaction can lead to a complex equilibrium involving several reactions giving off hydrogen and numerous by-products such as carbon oxides, methane, ethylene, acetaldehyde, acetone and coke [6,7] (Eqs. (2)–(15)).



* Corresponding author. Tel.: +39 089964147; fax: +39 089964057.

E-mail address: vpalma@unisa.it (V. Palma).



In this work, the thermodynamic analysis of the ESR reaction has received considerable attention, to provide guidelines for the selection of optimal operational parameters. The equilibrium composition of the gases, in the temperature range 100–1000 °C, has been calculated considering nine gaseous species, $\text{C}_2\text{H}_5\text{OH}$, H_2O , CH_4 , CO , CO_2 , H_2 , $\text{C}_2\text{H}_4\text{O}$, $\text{C}_3\text{H}_6\text{O}$, C_2H_4 and one in solid phase, carbon, as potential products. It is also assumed that the carbon formed is elemental, in the graphitic form, with a negligible vapour pressure in the overall analyzed temperature range. In this way, the amount of carbon can be included in the elemental mass balance [10].

Confirming the literature results, since the reaction takes place with an increase in the number of moles, the equilibrium conversion decreases as the reaction pressure increases. As a consequence, high pressure ESR is undesirable [11]. The effect of $\text{H}_2\text{O}/\text{EtOH}$ (S/E) ratio and reaction temperature on the equilibrium ethanol conversion showed that at $\text{S/E}=3$, the reaction reached nearly 100% ethanol conversion at temperatures higher than 577 °C. Excess H_2O improved the equilibrium conversion, reaching a value higher than 95% with $\text{S/E}=5$ at 277 °C, and reducing the yield of undesirable products such as CO , CH_4 and carbon [12]. Carbon formation occurs only at low water to ethanol ratios (<2) and low temperatures (<600 °C) [13].

At temperatures higher than 600 °C the ESR is thermodynamically favoured, but it is also promoted the formation of a large amount of CO , which is a poison for the PEM fuel cells. [14,15]. As a consequence, the water gas shift (WGS) reaction (Eq. (14)) must be performed in one or more later steps on the reformate, to purify hydrogen from CO . Thus high temperature operations raise an obvious concern over the energy efficiency of the ESR, as well as the overall energy cycle [16–18].

As a result, it is of great interest to lower the ESR reaction temperature, with the objective of minimizing both the CO formation and the thermal duty [19,20]. Several recent papers have proposed different process loops options at low temperatures [21,22]. In many cases, it has also been considered to assemble the functions of the traditional reformer and the gas cleaning unit into a membrane reactor (MR) [23,24].

Nevertheless, at temperatures lower than 600 °C, the hydrogen yield strongly decreases, since the conditions are in favour of the formation of unwanted by-products, which may in turn be coke precursors [25]. The efficiency of hydrogen production from ESR depends on the control of the formation of these products. Therefore, a properly designed catalysts for the steam reforming of ethanol at low temperature (LT-ESR) is important, to achieve high efficiency and selectivity for hydrogen production [18].

Both noble metals (e.g., Pd , Pt , Ru , Rh) and non-noble metals (e.g., Co , Ni , Cu) have been studied for ESR reaction [26–28]. Some preliminary works have been published recently on the use of $\text{Rh}/\text{Al}_2\text{O}_3$, $\text{Ni}/\text{La}_2\text{O}_3$, ZnO , $\text{Co}/\text{Al}_2\text{O}_3$, Cu/SiO_2 combined with

Ni/MgO , Cu , Ni , Pt , or Rh on various supports, potassium promoted Ni/Cu , and dual bed Pd/C $\text{Ni}/\text{alumina}$ systems [29–32].

The catalytic performance of supported noble metal catalysts has been investigated with respect to the nature of the active metallic phase (Rh , Ru , Pt , Pd), the nature of the support (Al_2O_3 , MgO , TiO_2) and the metal loading. $\text{Rh}/\text{CeO}_2\text{-ZrO}_2$ is very active for ESR at low temperature (450 °C) [33,34], and for low-loaded catalysts, seems to be more active and selective towards hydrogen formation compared to Ru , Pt and Pd . Rhodium is also resistant to sintering among the oxide-supported noble metals catalysts for ethanol reforming [14,35–41] but its performance is strongly dependent on oxide support. Platinum is considered very promising for the ethanol reforming to hydrogen, even if typically promoted via ethanol decomposition and dehydration [41]: it is possible to take advantage of the natural aptitude of Pt for the CO removal, enhancing its activity and selectivity by using the synergic effect of Co or Ni [11]; on the other hand, the activity of platinum in WGS reaction can be used to improve to catalytic performance of other metals.

Among the non-noble metals, cobalt and nickel are very common active species for the desired reactions [42–45]. Nickel catalysts are well known for their activity in reforming reactions and low cost. However, they have a troublesome problem, such as deactivation tendency, due to a high coke deposition. As a result, catalysts have been developed that limit the coke formation; i.e., Ni supported on Y_2O_3 , La_2O_3 and CeO_2 to reduce carbon deposition, and ZrO_2 with Y_2O_3 and La_2O_3 for CO reduction, [45] or $\text{Cu}/\text{Ni}/\text{K}/\text{Al}_2\text{O}_3$ [46–48] and $(\text{Ni}/\text{La}_2\text{O}_3)/\text{Al}_2\text{O}_3$ [49,50] for enhancing activity and long-term stability for hydrogen production.

In the present study the reaction of ethanol steam reforming at temperature lower than 600 °C on a commercial CeO_2 -supported Pt/Ni catalyst has been carried out. The dependence of the catalytic activity and selectivity on the reaction temperature, the $\text{H}_2\text{O}/\text{C}_2\text{H}_5\text{O}$ molar ratio and the contact time were studied. Time on stream experiments were also performed in order to evaluate catalyst stability and coke formation. A preliminary kinetic approach was realized, leading to the mathematical modelling of the reaction pathway.

2. Experimental

2.1. Catalyst preparation and characterization

The catalyst 3 wt% Pt –10 wt% Ni/CeO_2 was prepared by calcination of commercially available CeO_2 (Aldrich, BET = 80 m²/g) at 600 °C (heating rate = 10 °C/min), followed by sequential wet impregnations using respectively, aqueous nickel acetate $\text{C}_4\text{H}_6\text{O}_4\text{Ni}\cdot 4\text{H}_2\text{O}$ (Aldrich) and platinum chloride PtCl_4 (Carlo Erba Reactants) solutions, with an intermediate and a final calcination at 600 °C.

The metal load has been previously optimized through a preliminary screening of different relative amounts of the noble and non-noble metal in the range 1–5 wt.% as Pt and 5–20 wt.% as NiO respectively [51].

The effective metal load was determined through the Energy Dispersive X-Ray Fluorescence (EDXRF) analysis (Thermo-Scientific QUANT'X). The specific surface area (SSA) was determined by N_2 adsorption-desorption isotherm at –196 °C (B.E.T. method) after a pre-treatment at 150 °C for 1 h in He flow, with a Costech Sorptometer 1040. The crystallites phases were detected through X-Ray Diffraction (XRD) technique, using a D-max-RAPID X-ray microdiffractometer, with a cylindrical imaging plate detector. Before each ethanol steam reforming test, the catalyst underwent a temperature programmed reduction (TPR) in situ under 1000 cm³/min (STP) flow rate of a gas mixture containing 5 vol.% of H_2 in N_2 , from RT to 600 °C with a 10 °C/min

heating rate. Several characterization techniques were applied on the used samples: the TGA-MS, were performed through TA Instrument Q600 coupled with PFEIFFER ThermoStar Quadrupole Mass Spectrometer; the Laser Raman spectroscopy, with a Dispersive MicroRaman (Invia, Renishaw), equipped with 785 nm diode-laser, in the range 100–2500 cm⁻¹ Raman shift; Temperature Programmed Desorption (TPD) experiments after ethanol adsorption helped to hypothesize the role of the ethanol in the reaction. The adsorption of 10 vol.% of ethanol in N₂ flow (Total flow rate = 1000 cm³/min (STP)) was realized at 40 °C. The desorption in N₂ flow was performed, with a heating rate of 10 °C/min, up to 600 °C.

2.2. Catalytic tests

The catalytic tests were performed in an experimental set-up, previously reported and described in details [25].

All the gases employed in this work come from SOL S.p.A with a purity degree of 99.999%.

The gases for the TPR, TPD and ESR experiments are fed through Brooks 5850 mass flow controllers (MFC) while the mixture of bidistilled water and hi-purity ethanol, stored in a 2 bar nitrogen pressurized tank, is fed through a Coriolis controller (Quantum by Brooks). The water/ethanol mixture, premixed with the dilution nitrogen, is sent to a boiler to be vaporized. All the lines after the boiler are heated and controlled at 140 °C.

After vaporization, the feed mixture is sent to the reactor, a tubular stainless steel (AISI-310) reactor, operating isothermally at atmospheric pressure. The catalytic bed, realized by sandwiching the powder catalyst (180–355 mm) between quartz flakes, is located in the annular section of the reactor (18 mm i.d.), placed in a three zone electric oven. The oven control is realized by three temperature programmer-controller (TLK 43 by Tecnologic) connected to three type K thermocouple located inside the oven. Three other "K type" thermocouples were used to measure the temperature of the catalytic bed inside the reactor; in particular, in correspondence of the inlet, the middle and the outlet of the catalytic bed. The pressure drops through the catalytic bed were also continuously monitored by a differential pressure sensor.

The reactor outlet concentrations of C₂H₅OH, H₂O, CH₄, CO, CO₂ and other by-products are monitored with an on line Nicolet Antaris IGS FT-IR multi-gas analyser, able to simultaneously analyze and display more than 30 gases. The analyser is equipped with a heated gas cell, specifically designed with an optical path length of 12 cm, operating at temperature up to 185 °C and a MCT-A N₂ liquid cooled detector. The data were acquired at 0.5 cm⁻¹ and cell temperature and pressure were monitored and used to correct gas concentrations. To avoid any condensation, all connection from feed section to FT-IR gas analyser was heated and controlled at 140 °C. After a cold trap for gas conditioning at 3 °C, H₂ and O₂ are analyzed by a thermoconductivity ABB-CALDOS 27 and a continuous paramagnetic analyser ABB-MAGNOS 206, respectively. All data are monitored using a Labview interface on a personal computer connected to the analysers.

As a first approach, the catalytic tests were performed with a simulated bio-ethanol mixture, obtained by mixing bidistilled water and pure ethanol, according to the desired water/ethanol ratio, without considering the effect of contaminants like methanol and diethyl ether. The catalytic activity and selectivity tests were performed at a fixed water-to-ethanol molar ratio, defined as r.a. = $\frac{\text{moles H}_2\text{O}}{\text{moles EtOH}}$, equals to 3. It was selected from a thermodynamic analysis, considering that it is the minimum value to avoid coke formation. It has to be pointed out that, in reality, bio-ethanol is a mixture containing a water/ethanol molar ratio of 29.0/1–18.7/1 [19]. The dilution ratio, defined as r.d. = $\frac{\text{moles N}_2}{\text{moles C}_2\text{H}_5\text{OH} + \text{moles H}_2\text{O}}$,

Table 1
Results of XRF, N₂ adsorption and XRD analysis.

Catalyst	Metals content (%)		SSA (m ² /g)	dCeO ₂ (nm)	dNiO (nm)
	Pt	Ni			
CeO ₂				60	17
Pt-Ni/CeO ₂	2.8		9.8	42	23
					21

was equals to 4. In these conditions, the feed composition is 5 vol.% of ethanol/15 vol.% of water/80 vol.% of nitrogen.

The temperature range was 250–600 °C, and the GHSV one was 7500–15,000 h⁻¹. These selected parameters are very severe, in terms of reaction temperature, ethanol concentration and water content in the feed stream. These are not the favoured conditions from the thermodynamic point of view; probably for these reasons, in literature the studies are mainly focused on the high temperature range and, when performed at lower temperature, very diluted conditions and high r.a. ratios are used [13–15].

The catalytic performance was evaluated through the conversion of ethanol X_{EtOH}, the conversion of water X_{H₂O}, the selectivity towards the main products S_{H₂}, S_{CH₄}, S_{CO}, S_{CO₂}, S_{C₂H₄O}, S_{C₂H₄}, S_{C₄H₆O}, S_C and the hydrogen yield Y_{H₂} (Eqs. (16)–(24))

$$X_{\text{EtOH}} = \frac{(\text{moles}_{\text{EtOH,in}} - \text{moles}_{\text{EtOH,out}})}{\text{moles}_{\text{EtOH,in}}} \times 100 \quad (16)$$

$$S_{\text{H}_2} [\%] = \frac{\text{moles}_{\text{H}_2}/6}{(\text{moles}_{\text{EtOH,in}} - \text{moles}_{\text{EtOH,out}})} \times 100 \quad (17)$$

$$S_{\text{CO}} [\%] = \frac{\text{moles}_{\text{CO}}/2}{(\text{moles}_{\text{EtOH,in}} - \text{moles}_{\text{EtOH,out}})} \times 100 \quad (18)$$

$$S_{\text{CO}_2} [\%] = \frac{\text{moles}_{\text{CO}_2}/2}{(\text{moles}_{\text{EtOH,in}} - \text{moles}_{\text{EtOH,out}})} \times 100 \quad (19)$$

$$S_{\text{CH}_4} [\%] = \frac{\text{moles}_{\text{CH}_4}/2}{(\text{moles}_{\text{EtOH,in}} - \text{moles}_{\text{EtOH,out}})} \times 100 \quad (20)$$

$$S_{\text{C}_3\text{H}_6\text{O}} [\%] = \frac{\text{moles}_{\text{C}_3\text{H}_6\text{O}}/(2/3)}{(\text{moles}_{\text{EtOH,in}} - \text{moles}_{\text{EtOH,out}})} \times 100 \quad (21)$$

$$S_{\text{C}_2\text{H}_4\text{O}} [\%] = \frac{\text{moles}_{\text{C}_2\text{H}_4\text{O}}}{(\text{moles}_{\text{EtOH,in}} - \text{moles}_{\text{EtOH,out}})} \times 100 \quad (22)$$

$$S_{\text{C}} [\%] = \frac{\text{moles}_{\text{C}}/2}{(\text{moles}_{\text{EtOH,in}} - \text{moles}_{\text{EtOH,out}})} \times 100 \quad (23)$$

$$Y_{\text{H}_2} [\%] = \frac{\text{moles}_{\text{H}_2,\text{out}}}{6(\text{moles}_{\text{EtOH,in}})} \times 100 \quad (24)$$

The operating conditions of the time on stream (TOS) tests were selected with the seek of enhancing the possible coking reactions, thus better evaluating the catalyst stability. For this reason, at GHSV = 15,000 h⁻¹, it was used a critical temperature (T = 450 °C) and a very concentrated feed stream (10 vol.% of ethanol) [52,53].

Before the development of a mathematical model, able to simulate the reaction pathway on the catalyst Pt/Ni, the effect of contact time on the products distribution was investigated in the range 0–600 ms, at different temperatures, in the range 350–500 °C, and water to ethanol molar ratio = 6.

3. Results and discussion

3.1. Catalyst characterization before the ESR reaction

The experimental metal load obtained by XRF analysis was in agreement with the nominal content, as reported in Table 1. The result of SSA measurement, reported in the same table, showed that the deposition of the active species causes a specific surface area

Table 2
TPR H₂ uptake of Pt–Ni/CeO₂ catalyst.

Catalysts	T (°C)	H ₂ uptake (mmol/g _{cat})				
		Experimental	Expected Pt ⁴⁺ → Pt ⁰	Expected Ni ²⁺ → Ni ⁰	Total experimental	Total expected
Pt/Ni	168	480	308			1985
	288	856				2015
	319	649		1707		

decrease with respect to the pure support, probably due to crystallites rearrangement and the metals–support interaction during impregnation and calcination steps [54].

XRD diffractograms of calcined support and catalyst samples have been compared with the database of the International Centre for Diffraction Data (ICDD). Only peaks of the fluorite structure of the cerium oxide, and the signals related to NiO formed during calcination (ICDD file: 78-0643) was detected, while no peak relevant to Pt or PtO_x species was visible from the spectra, likely owing to the low metal content and/or to a good Pt dispersion, promoted by ceria [55]. The average size *d* of the oxides crystallites was calculated through Scherrer formula and reported in Table 1.

In particular, the dimension of the NiO crystallites was calculated at 43.298° on (200) crystal plane diffraction while the dimension of the cerium oxide crystallites for each catalyst was obtained as the average between the value calculated for the peak at 28.542°, 47.475° and 56.332° corresponding to diffractions planes (1 1 1) (2 2 0) (3 1 1), respectively.

The TPR-H₂ measured profile of Pt/Ni/CeO₂ catalyst is reported in Fig. 1. The profile was deconvoluted after background subtraction by a least-squares fitting to Gaussian–Lorentzian functions using the software Microcal Origin. According to literature, the peak at lower temperature (about 168 °C) can be ascribed to the PtO₂ species reduction, while the peaks at higher temperature (288 and 319 °C) can be attributed to NiO reduction [52,56]. Considering the metal loading of the sample, the theoretical hydrogen uptake due to the overall reduction of Pt⁴⁺ to metallic Pt has been calculated equals to 308 μmol/g_{cat} and the hydrogen uptake due to the reduction of the NiO to metallic Ni equals to 1707 μmol/g_{cat}. The calculation of the overall H₂ uptake is in good agreement with the experimental values, as shown in Table 2, whereas the single contributions are slightly different from the expected ones: in particular, the H₂ uptake due to PtO_x species reduction is higher than the theoretical one even as the H₂ uptake due to nickel oxide reduction is lower than the expected one. This effect can be due to the H₂-spillover phenomenon promoted by the noble metal,

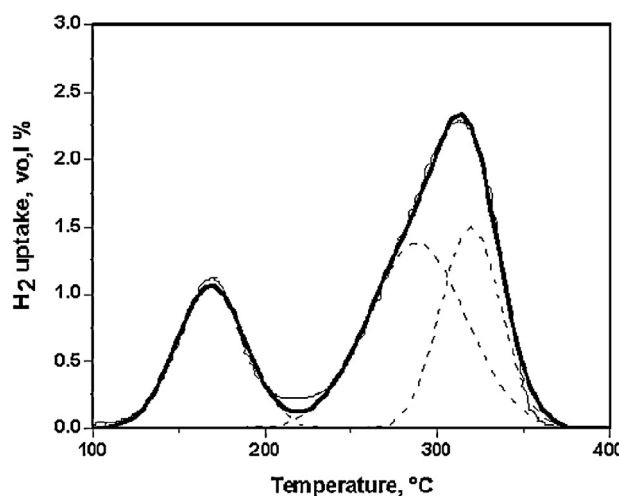


Fig. 1. TPR profile with peaks deconvolution of Pt–Ni/CeO₂ catalyst.

that enhance the reduction at lower temperatures of the free NiO particles dispersed on the support surface [57].

3.2. Catalytic activity and selectivity tests

The catalytic tests were carried out in the following operating conditions:

- Total flow rate = 1000 cm³/min (STP);
- GHSV = 15,000 h⁻¹
- Temperature = 250–600 °C.
- r.d. = 4;
- r.a. = 3.

These conditions correspond to the following feed composition 5 vol.% EtOH/15 vol.% H₂O/80 vol.% N₂, and a contact time of about 240 ms.

The catalytic performance of the Pt/Ni sample for the ESR reaction is very promising, especially concerning H₂ production and ethanol conversion. In Fig. 2(a), there is the products distribution for the Pt/Ni sample as a function of temperature, in comparison with the equilibrium values. The experimental values are in very good agreement with the thermodynamic calculations in the overall temperature range, yet at the low contact time of 240 ms. The carbon mass balance is closed up to 99%, when considering C₂H₅OH, CO, CH₄ and CO₂ as C-containing products.

Fig. 2(b) shows for the same sample and test conditions, the results in terms ethanol conversion (*X*_{C₂H₅OH}), hydrogen yield (*Y*_{H₂}) and products selectivity (*S*_{CH₄}, *S*_{CO}, *S*_{CO₂}) vs. temperature. The ethanol is completely converted, yet at *T* of about 290 °C, and the performances, in terms of H₂ yield, improves with temperature. The CH₄ selectivity showed an opposite trend, and decrease with temperature.

3.3. Time on stream tests

The TOS tests were performed in the following conditions:

- GHSV = 15,000 h⁻¹;
- r.d. = 1.5;
- r.a. = 3.
- *T* = 450 °C.

These conditions of low temperature and very low steam to ethanol ratio are particularly severe, and were specifically chosen to enhance the coke formation and the catalyst deactivation phenomena.

The results of the TOS test on the Pt/Ni sample are reported in Fig. 3: after 300 min of time on stream there was no appreciable change in the products distribution (Fig. 3a), in particular in the hydrogen production, suggesting the absence of detectable catalyst deactivation phenomena. On the other hand, during the same time a sensible increase in the pressure drops occurs from the initial values of about 10 mbar to a final value higher than 1 bar (Fig. 3b).

This effect can be likely ascribed to the reactor plugging, typically related to the sintering and/or coking phenomena probably

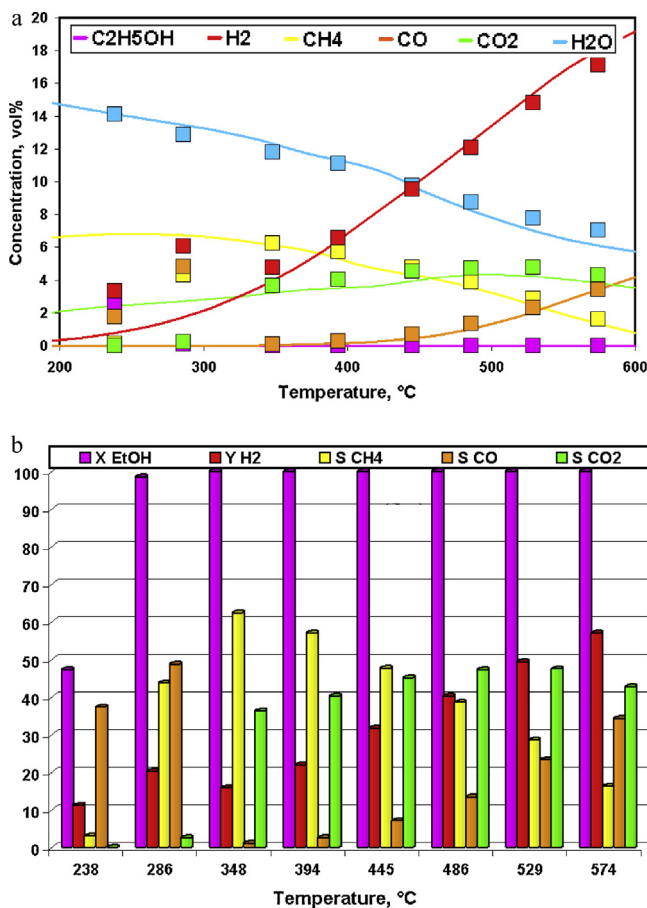


Fig. 2. (a) Experimental (points) and equilibrium (line) products distribution as a function of temperature for Pt/Ni catalyst. (b) Ethanol conversion ($X_{C_2H_5OH}$), hydrogen yield (Y_{H_2}) and products selectivity (S_{CH_4} , S_{CO} , S_{CO_2}) as a function of temperature for Pt/Ni catalyst. (Total flow rate = 1000 N cm³/min; GHSV = 15000 h⁻¹; r.d. = 4; r.a. = 3).

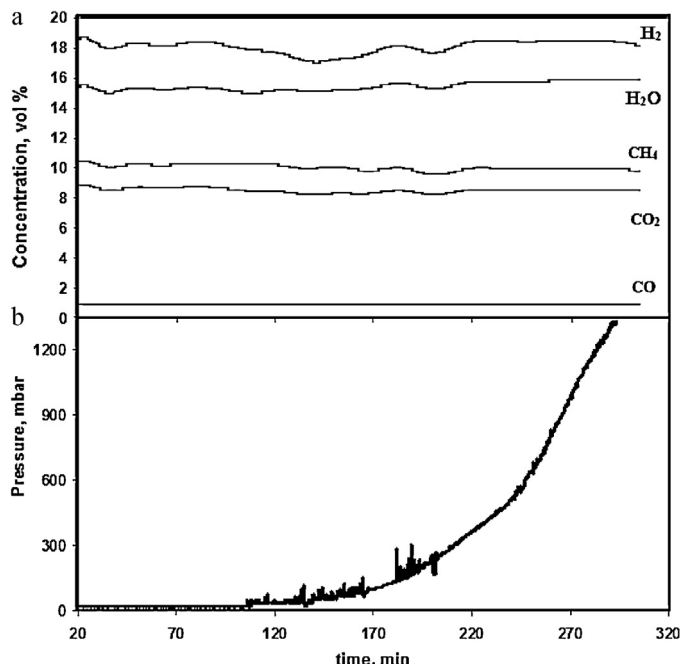


Fig. 3. (a) Experimental product distribution and pressure drop (b) as a function of time during the stability test in concentrated catalytic tests for Pt/Ni catalyst. (Total flow rate = 1000 N cm³/min; GHSV = 15000 h⁻¹; r.d. = 1.5; r.a. = 3).

caused by accumulation of carbonaceous species in the catalytic bed.

3.3.1. Catalyst characterization after the TOS tests

Some characterizations after the time on stream test were carried out, in order to verify if sintering and/or coking phenomena are accountable for this behaviour.

From XRD analysis on the used sample, no considerable variation is evidenced in the dimensions of CeO₂ and NiO crystallites, excluding any sintering phenomena. On the other hand, the absence of sintering effect of Pt cannot be evidenced, due to the absence of any signal related to these substance, both in the fresh and used sample.

On the contrary, a considerable increase in the SSA value of the same after the TOS test was noticed, changing from 40 to 60 m²/g. This could be likely related to the formation of micro-porosity into the catalyst particles and/or the presence of some solid species characterized by a higher SSA, i.e. carbonaceous compounds. The deposition of coke on the catalyst surface was also confirmed by the Raman spectrum of the sample after the time on stream test: supporting the previous findings, it was possible to detect the intense peak at a Raman shift of about 1350 cm⁻¹, index of the presence of crystalline graphite carbon, and the peak at about 1590 cm⁻¹, ascribed to amorphous carbon with defects in curved graphene sheet and finite size of tubes crystalline domains [53].

In addition, from TGA-MS analysis after the time on stream test, it was measured a weight loss of about 3.4% in the range 400–600 °C, corresponding to the CO₂ formation in the gas phase and observed in the MS data for the $m/z = 44$, confirming the presence of carbonaceous compounds on the used sample. This technique was also applied to quantify the carbon amount on the catalyst surface, allowing so to evaluate the “carbon selectivity” that indicate the percentage of the overall carbon fed during the test that was converted to coke. For the previous test relevant to the Pt/Ni sample, a very low carbon selectivity of about 0.6% was calculated, thus not quantifiable from the carbon mass balances and not able to deactivate the active sites during the test time, since the catalyst activity and selectivity for the H₂ production reaction remains practically unchanged during the TOS tests.

In addition, the coke formation tendency could be further reduced by changing the operating conditions. For instance, the TOS test was also performed at r.a. = 6, showing that, by increasing the water-to-ethanol molar ratio, the coke formation rate was lower, and the time required to reach 1 bar of pressure drop was about doubled becoming higher than 600 min. In this case the SSA value does not significantly change after the TOS test and the coke selectivity is lower. This positive effect could be likely due to the higher steam gasification rate of the coke precursors compounds, enhanced by the higher steam concentration and the oxygen vacancies of the catalytic support [58].

Therefore, the net coke formation rate is the difference between the coke formation rate and the coke gasification rate [58]. The first one strongly depends on the ethanol concentration, the carbon source, and on the catalyst properties, while the second one is related to the amount of steam in the feed stream and to the role of the catalytic support, like the oxygen vacancies [59]. Therefore, considering that the water-to-ethanol molar ratio in the raw bio-ethanol is greatly higher [19], the results here reported appears even more promising.

From the TGA-MS tests on the used samples, the coke formation rates were also calculated: they are among the lowest of the recent scientific literature, as evident from Table 3. It is also important to note that among all the samples listed in the table, the lower coke formation rates were obtained at higher temperatures and/or in more diluted conditions compared to our tests [42,60–69], so

Table 3
Coke formation rates.

Catalyst	Deactivation test conditions	Deactivation rate ($g_c/(g_{cat} h)$)	Ref.
$Ce_2Zr_{1.5}Co_{0.47}Rh_{0.07}O_{8-\delta}$	$T = 550^\circ C, H_2O/EtOH = 6, EtOH$ volum. Conc. = 4.3%, GHSV = 26,000 h ⁻¹ (140 ms)	0.00022	[60]
9%Co/ZnAl	$T = 500^\circ C, H_2O/EtOH = 3.7, EtOH$ volum. Conc. = 3%	0.0025	[61]
9%Co/ZnAl	$T = 600^\circ C, H_2O/EtOH = 3.7, EtOH$ volum. Conc. = 3%	0.00525	[60]
25%Co/ZnAl	$T = 500^\circ C, H_2O/EtOH = 3.7, EtOH$ volum. Conc. = 3%	0.003	[60]
25%Co/ZnAl	$T = 600^\circ C, H_2O/EtOH = 3.7, EtOH$ volum. Conc. = 3%	0.00175	[60]
8%Co/Al ₂ O ₃	$T = 400^\circ C, H_2O/EtOH = 3, EtOH$ volum. Conc. = 13%	2.7334	[61]
8%Co/SiO ₂	$T = 400^\circ C, H_2O/EtOH = 3, EtOH$ volum. Conc. = 13%	1.5778	[61]
18%Co/MgO	$T = 400^\circ C, H_2O/EtOH = 3, EtOH$ volum. Conc. = 13%	1.889	[61]
0.11%Fe–5%Co/SiO ₂	$T = 550^\circ C, H_2O/EtOH = 5, EtOH$ volum. Conc. = 8.5%	0.052	[63]
0.22%Fe–5%Co/MgO	$T = 550^\circ C, H_2O/EtOH = 5, EtOH$ volum. Conc. = 8.5%	0.01367	[63]
0.22%Fe–5%Co/SrTiO ₃	$T = 550^\circ C, H_2O/EtOH = 5, EtOH$ volum. Conc. = 8.5%	0.02834	[63]
0.22%Fe–5%Co/α-Al ₂ O ₃	$T = 550^\circ C, H_2O/EtOH = 5, EtOH$ volum. Conc. = 8.5%	0.017	[63]
0.11%Fe–5%Co/α-Al ₂ O ₃	$T = 550^\circ C, H_2O/EtOH = 5, EtOH$ volum. Conc. = 8.5%	0.021	[63]
10%Co/SiO ₂	$T = 550^\circ C, H_2O/EtOH = 3, EtOH$ volum. Conc. = not sp.	0.004	[64]
10%Co/γ-Al ₂ O ₃	$T = 550^\circ C, H_2O/EtOH = 3, EtOH$ volum. Conc. = not sp.	0.002	[64]
5%Ni/10%La ₂ O ₃ –ZrO ₂	$T = 700^\circ C, H_2O/EtOH = 4.84, EtOH$ volum. Conc. = not sp.	0.00045	[61]
5%Co/10%La ₂ O ₃ –ZrO ₂	$T = 700^\circ C, H_2O/EtOH = 4.84, EtOH$ volum. Conc. = not sp.	0.000125	[65]
20%Ni/SiO ₂ (Citric Acid/Nichel = 0.5)	$T = 600^\circ C, H_2O/EtOH = 3.5, EtOH$ Mass. Conc. = 9.8%	0.0035	[66]
20%Ni/SiO ₂ (Citric Acid/Nichel = 1)	$T = 600^\circ C, H_2O/EtOH = 3.5, EtOH$ Mass. Conc. = 9.8%	0.0045	[66]
20%Ni/SiO ₂ (Citric Acid/Nichel = 1.5)	$T = 600^\circ C, H_2O/EtOH = 3.5, EtOH$ Mass. Conc. = 9.8%	0.016	[66]
20%Ni/SiO ₂ (Citric Acid/Nichel = 2)	$T = 600^\circ C, H_2O/EtOH = 3.5, EtOH$ Mass. Conc. = 9.8%	0.0265	[66]
20%Ni/SiO ₂ (Citric Acid/Nichel = 3)	$T = 600^\circ C, H_2O/EtOH = 3.5, EtOH$ Mass. Conc. = 9.8%	0.0375	[66]
Cu–Ni/SiO ₂	$T = 700^\circ C, H_2O/EtOH = 3.7, EtOH$ volum. Conc. = 0.053%	0.1534	[67]
Ni–Al/SiO ₂	$T = \text{not specified}, H_2O/EtOH = 3.7, EtOH$ volum. Conc. = 0.053%	0.1	[68]
10%Co/CeO ₂	$T = 500^\circ C, H_2O/EtOH = 3, O_2/EtOH = 0.5, EtOH$ vol. Conc. = 0/18.75%	0.0081 (average)	[69]
25%Cs _{0.05} Ni _{0.95} /ZrO ₂	$T = 500^\circ C, H_2O/EtOH = 13, EtOH$ volum. Conc. = 0.5%	0.0156	[42]
25%La _{0.2} Ni _{0.8} /ZrO ₂	$T = 500^\circ C, H_2O/EtOH = 13, EtOH$ volum. Conc. = 0.5%	0.0094	[42]
3%Pt/10%Ni/CeO ₂	$T = 450^\circ C, H_2O/EtOH = 3, EtOH$ volum. Conc. = 5%	0.00675	Our work
3%Pt/10%Ni/CeO ₂ (IMP)	$T = 450^\circ C, H_2O/EtOH = 6, EtOH$ volum. Conc. = 5%	0.004542	Our work

in a more favourable condition where the coke gasification rate is higher, as very well-known [58].

3.4. Preliminary kinetic evaluation

The kinetic behaviour of the catalyzed LT-ESR reaction was studied on the Pt/Ni sample analysing the products distribution at different contact time values in the range 0–600 ms and at different temperatures in the range 350–500 °C.

The objectives of these experimental campaigns were to identify the main reactions involved in the reaction pathway, and realize a mathematical model, able to simulate the “reaction pathway” over Pt/Ni.

3.4.1. Evolution of the products distribution vs temperature and contact time

The behaviour of the products distribution at 370 in the range 0–600 ms is reported in Fig. 4. Each experimental data at a fixed contact time is a stationary value at the reactor outlet. At very low contact time (Fig. 4a), for values lower than 4 ms, no ethanol and steam conversion is obtained. This could be an index of a characteristic time for the adsorption of the reactants before activating the reaction. Few ms later, only the acetaldehyde appears in the gas phase, and simultaneously the ethanol concentration decreases. Starting by 8 ms, the hydrogen is revealed in the gas phase, together with the CH₄ and CO about at the same values, and a lower CO₂ concentration. It is important to evidence that the CO profile reaches a maximum at about 16 ms, after that decreases, while the CO₂ and H₂ still increase, in very good agreement with the stoichiometry of the water gas shift reaction (Eq. (13)). In the range 20–45 ms, CO, CO₂, CH₄ and H₂ still increase while C₂H₅OH and C₂H₄O was totally converted. Up to about 100 ms (Fig. 4b), the H₂ concentration and the H₂O uptake increasing simultaneously, where a maximum is observed for CO₂ and H₂. After this point, another reaction happens between the CO₂ and the H₂ to drive the system to the equilibrium composition. In fact, in the

range 100–400 ms the concentration changes in the gas phase are in very good agreement with the stoichiometry of the methanation reaction (Eq. (15)) clearly indicating that this reaction occurs. At a contact time of about 400 ms, the gaseous composition is in agreement with the equilibrium and by analysing the system composition at higher contact times, any changes in the products distribution can be noticed. This evolution of products distribution suggest of a set of subsequent reactions, that are activated at different contact times.

The results at different temperatures are reported in Fig. 5. At 340 °C, the trend is similar to the results at 370 °C, even if the contact times of concentration peaks for each component appear different. In particular, acetaldehyde shows a maximum at 12 ms and CO at 32 ms. The peculiarity is that, by increasing the contact time up to 140 ms, the concentration of H₂, CO₂ and CH₄ progressively increase while H₂O decreases. At higher contact times, any change is evident in the products distribution and H₂ concentration is firmly higher than the expected one by equilibrium calculations. This is probably related to the very low temperature, at which the Pt/Ni catalyst is not yet able to activate the methanation reaction to drive the system to the thermodynamic equilibrium.

At 430 °C the system reaches the equilibrium conditions and the concentrations of CH₄, CO and C₂H₄O have a maximum at higher contact times: 24, 6 and 2 ms, respectively.

At 480 °C, the trend is similar to the previous temperature investigated but the time required to reach the equilibrium values lower. When the contact time increases, thus proceeding along the reactor, the ethanol and water conversion, together with the H₂ and CO₂ concentrations progressively increase, up to the equilibrium values, reached at about 50 ms. On the other hand, CH₄ concentration increases until 16 ms, after that decreases of about 10% passing from 24 to 45 ms, suggesting that the MSR reaction occurs. The concentration of CO and C₂H₄O has a similar trend, with a maximum at 5 and 1 ms, respectively. Indeed in this case, acetaldehyde is converted within few milliseconds.

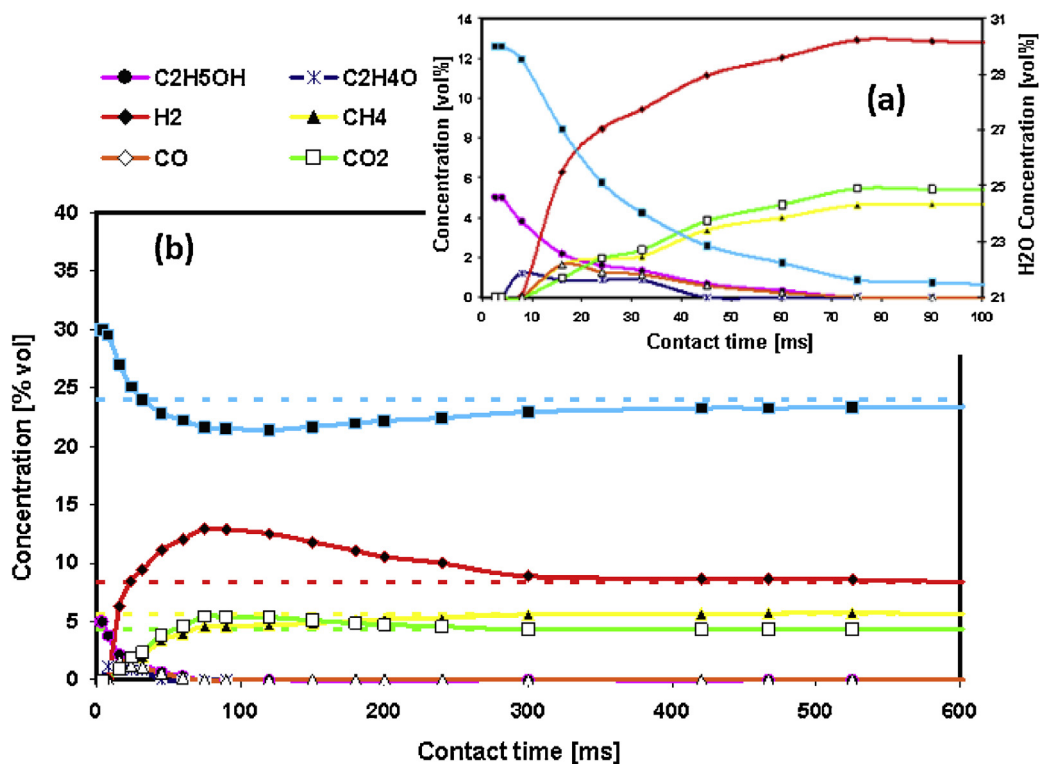


Fig. 4. Experimental (lines + points) and equilibrium (dotted lines) evolution of the products distribution vs contact time at 370 °C.

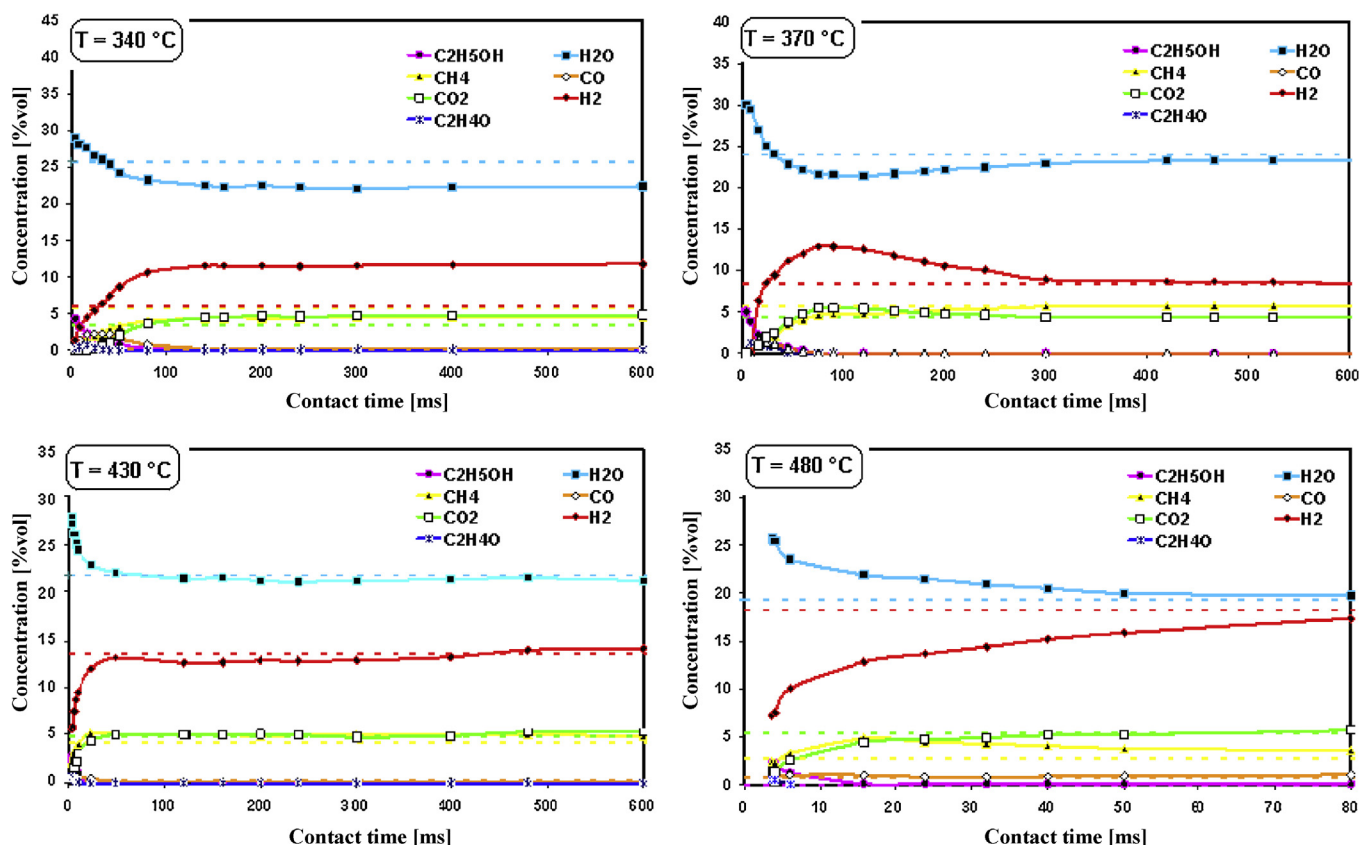


Fig. 5. Experimental (lines + points) and equilibrium (dotted lines) evolution of the products distribution vs contact time in the range 340–480 °C.

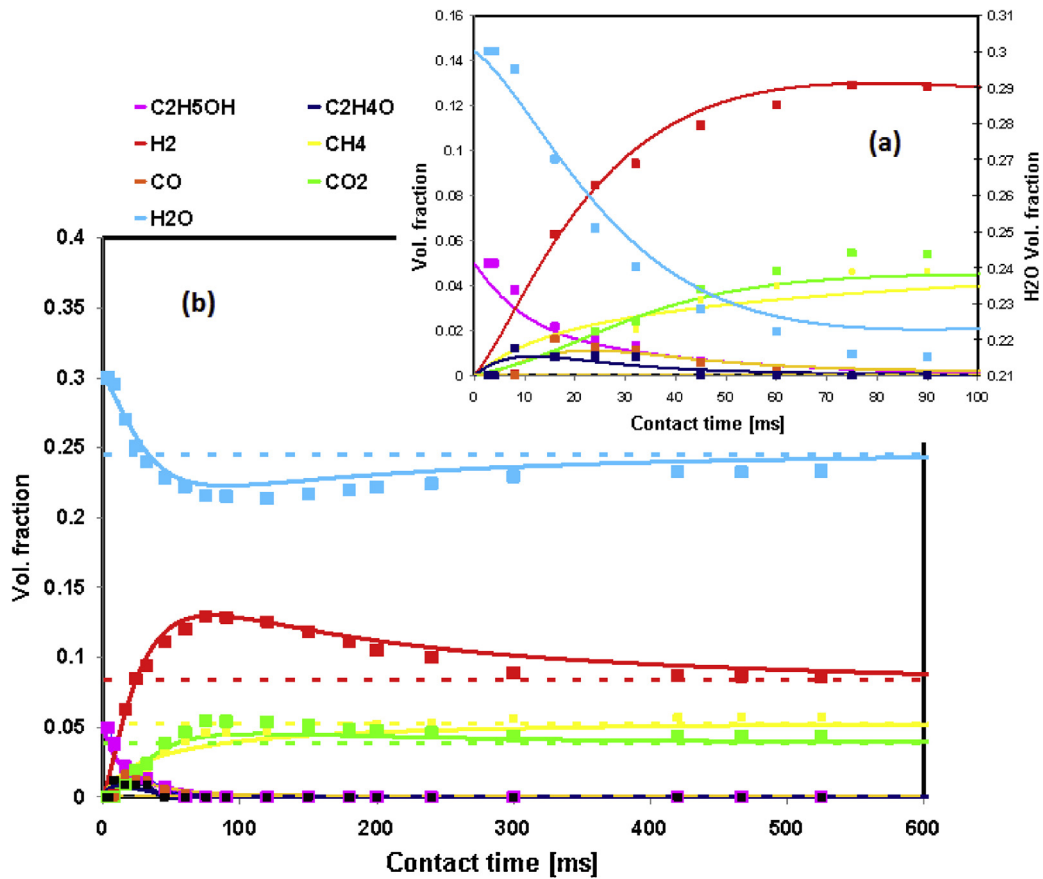


Fig. 6. Experimental (points), model (lines) and equilibrium (dotted lines) products distribution vs contact time at 370 °C.

The results of these tests and of the analysis of the recent literature suggested us to hypothesize the following set of reactions that can be considered also to develop the mathematical model:

- 1 ethanol dehydrogenation (Eq. (2)) [14,70–72];
- 2 ethanol decomposition (Eq. (11)) [73];
- 3 acetaldehyde decomposition (Eq. (3)) [70];
- 4 acetaldehyde steam reforming (Eq. (4)) [74];
- 5 water gas shift (Eq. (13)) [75];
- 6 CO₂-methanation (Eq. (15)) [28]

with the related kinetic expression for the reaction rates r_i , defined as a function of the partial pressures p_a :

$$r_1 = k_1 \left(p_{\text{EtOH}} - \frac{1}{K_{\text{eq}1}} p_{\text{Acet}} p_{\text{H}_2} \right) \quad (26)$$

$$r_2 = k_2 \left(p_{\text{EtOH}} - \frac{1}{K_{\text{eq}2}} p_{\text{CO}_2}^{0.5} p_{\text{CH}_4}^{1.5} \right) \quad (27)$$

$$r_3 = k_3 \left(p_{\text{Acet}} - \frac{1}{K_{\text{eq}3}} p_{\text{CO}} p_{\text{CH}_4} \right) \quad (28)$$

$$r_4 = k_4 \left(p_{\text{Acet}} p_{\text{H}_2\text{O}} - \frac{1}{K_{\text{eq}4}} p_{\text{CO}}^2 p_{\text{H}_2}^3 \right) \quad (29)$$

$$r_5 = k_5 \frac{K_{\text{ads CO}_2} K_{\text{ads H}_2\text{O}} \left(p_{\text{CO}} p_{\text{H}_2\text{O}} - \frac{1}{K_{\text{eq}5}} p_{\text{CO}_2} p_{\text{H}_2} \right)}{(1 + K_{\text{ads CO}} p_{\text{CO}} + K_{\text{ads H}_2\text{O}} p_{\text{H}_2\text{O}} + K_{\text{ads CO}_2} p_{\text{CO}_2})^2} \quad [76] \quad (30)$$

$$r_6 = k_6 \left(p_{\text{CO}_2} p_{\text{H}_2}^4 - \frac{1}{K_{\text{eq}6}} p_{\text{CH}_4} p_{\text{H}_2\text{O}}^2 \right) \quad (31)$$

where $k_1, k_2, k_3, k_4, k_5, k_6$ are the kinetic constants for each reaction, $K_{\text{eq}1}, K_{\text{eq}2}, K_{\text{eq}3}, K_{\text{eq}4}, K_{\text{eq}5}, K_{\text{eq}6}$ the equilibrium constants for each reaction, while $K_{\text{ads CO}}, K_{\text{ads H}_2\text{O}}, K_{\text{ads CO}_2}$ are the adsorption constants of the specified components.

For the optimization of the kinetic model, the adsorption constants are considered constants and equals to the average value in the range 300–500 °C [76]. In particular:

$$K_{\text{ads CO}} = 0.37 \text{ atm}^{-1}$$

$$K_{\text{ads H}_2\text{O}} = 80073.2 \text{ atm}^{-1}$$

$$K_{\text{ads CO}_2} = 1.701 \text{ atm}^{-1}$$

3.4.2. The mathematical model

The mathematical model was based on the hypothesis of an isothermal tubular plug flow reactor (PFR), with a fixed bed of catalyst; the sample density, experimentally measured, is 1.75 g/cc. The model equations were implemented in the software Microsoft Excel, Office 2010.

A total gas flow rate of 1000 cm³/min (STP) at atmospheric pressure is sent to the tubular reactor, with 5% vol.% of ethanol and 30 vol.% of steam in nitrogen.

The system was solved through n mass balance to the PFR, where n is the components number. The differential balances were:

$$\frac{dF_a}{dW} = - \sum_{j=1}^q v_{aj} * r_j \quad (32)$$

where a is an index of the component, j an index of the reaction, q the total number of the hypothesized reactions. To solve the seven differential equation (one for each component, expect nitrogen that

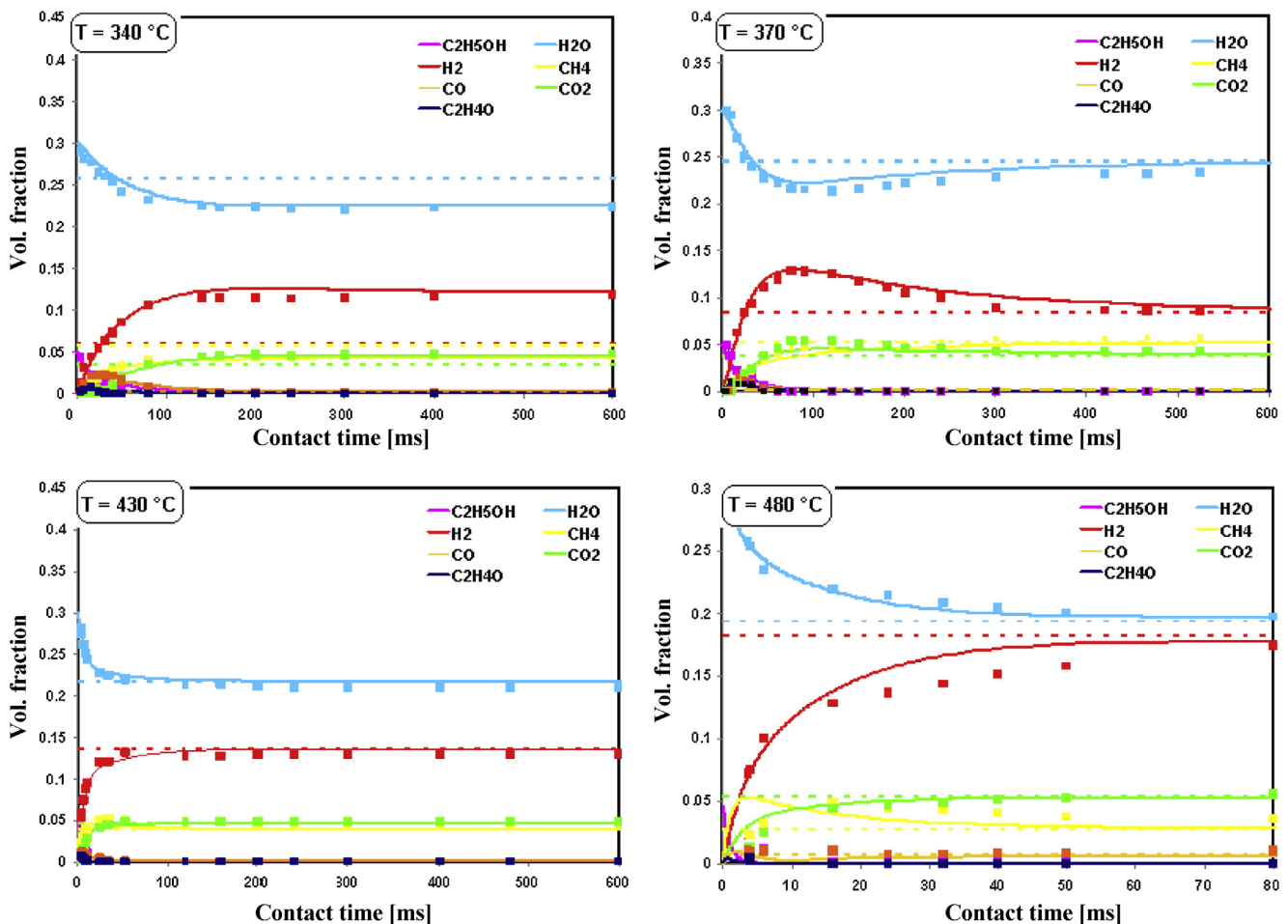


Fig. 7. Experimental (points), model (lines) and equilibrium (dotted lines) products distribution vs contact time in the range 340–480 °C.

is inert), the Euler method was used to integrate the system (Eq. (33)).

$$F_{a_{i+1}} = F_{a_i} - \sum_{j=1}^q (v_{aj} * r_j)_i * \Delta W \quad (33)$$

with $\Delta W = 0.001764583$ g, corresponding to a contact time of about 0.0605 ms.

After the solution of the mass balance, the results of the model were compared with the experimental values, through an objective function defined in Eq. (34).

$$f = \sum_{i=1}^n \sum_{j=1}^p (y_{\text{mod},j} - y_{\text{exp},j})_i^2 \quad (34)$$

where n is the components number, p the reactions number, y the molar fraction of the i component. This function should be maximized to obtain a minimum difference between experimental and model values, using the kinetic constants as the variable terms.

We decided to initially optimize the system at 370 °C, from which the evolution of the species seem more clearly linked to a possible reaction mechanism. The results of the optimization are shown in Fig. 6, in which there is volumetric composition of each component as a function of contact time.

There is a very good fitting of the experimental data, index that the hypothesized set of reaction is possible. In particular, acetaldehyde has a first maximum, indicating that the first reaction is the ethanol dehydrogenation to acetaldehyde (Eq. (2)), probably

simultaneously with the ethanol decomposition (Eq. (11)). Observing the increase of the CO, CH₄ and H₂ signal, it was possible to hypothesize that the following reactions are decomposition and steam reforming of acetaldehyde (Eqs. (3)–(4)). The decrease of CO and the increase of CO₂ are related to the water gas shift (Eq. (13)). The concentrations changes after 100 ms are in agreement with the stoichiometry of the CO₂ methanation (Eq. (15)): it has a very low kinetic since the hydrogen signal reaches a maximum at 90 ms, reaching the equilibrium at about 300 ms. The methanation is the last reaction step because it drives the system to the equilibrium and any other change is visible up to 600 ms. After the optimization, the model gives the values of the kinetic constants.

The results of the model are in agreement with the experimental data also at lower and higher temperatures, as shown in Fig. 7. At 340 °C, the model showed good results at all the contact times, confirming that, at this temperature, the Pt/Ni catalyst is not yet able to activate the methanation reaction, thus the system does not reach the equilibrium composition.

At 430 °C, it is noticeable that CH₄ has maximum and subsequently it decreases and this behaviour is different from the one at the previous temperature. This almost certainly means that the set of reactions is correct but the reaction mechanism is different.

At $T = 480$ °C, the products distribution of species like CH₄ and C₂H₄O is shifted at lower contact times, in comparison with the experimental trend. It is then possible that at higher temperatures other reactions are activated. In reality CH₄ has an evident maximum before reaching the equilibrium value, as a confirmation of a different mechanism.

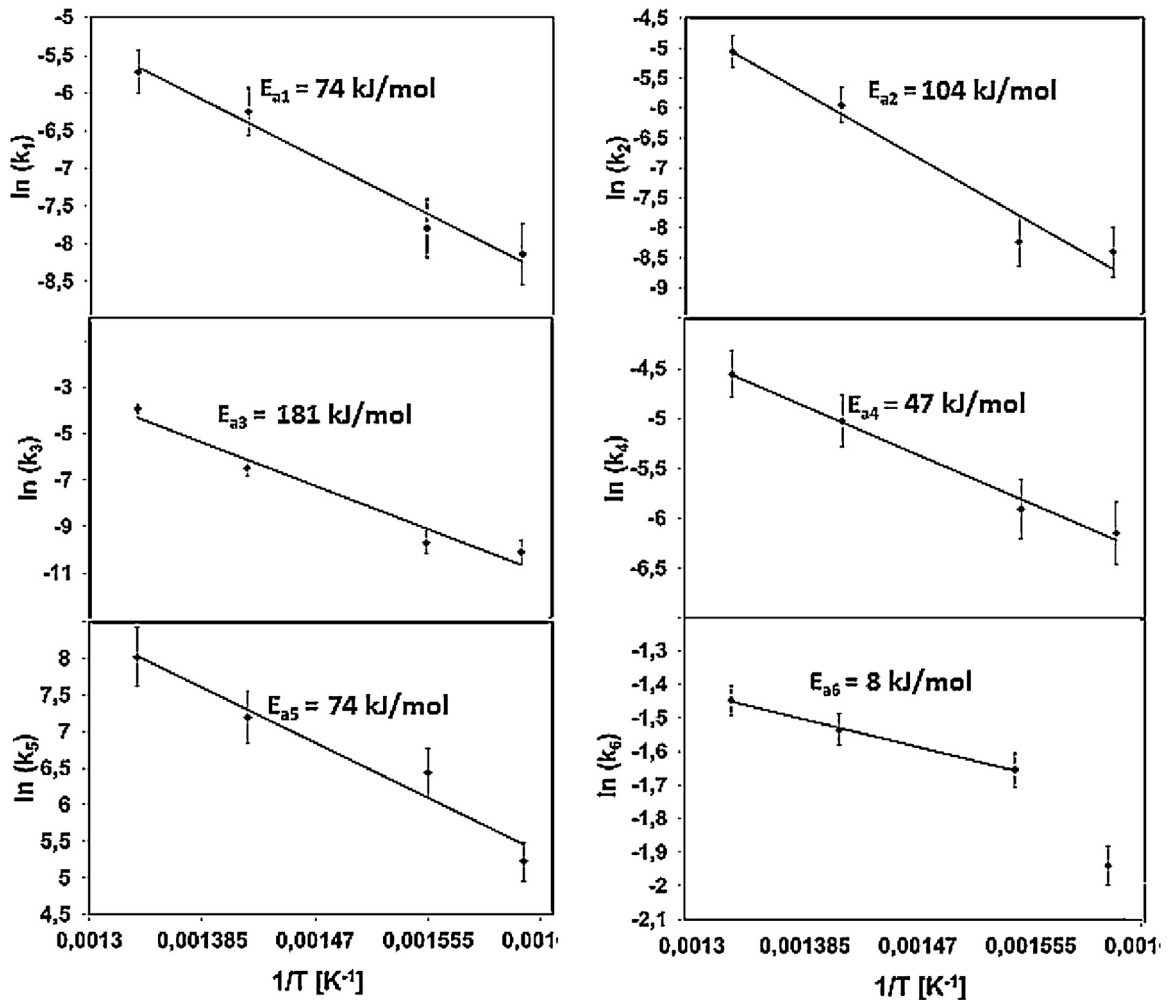


Fig. 8. Arrhenius plot for the kinetic constants of each reaction as a function of temperature.

3.4.3. Activation energy calculation

The activation energies E_{ai} of the reaction included in the mechanism were calculated starting from the kinetic constants achieved by the model at each temperature. The fitting was realized through the Arrhenius law, obtaining a coefficient of determination R^2 close to 1. The results related to each reaction as a function of temperature are plotted in Fig. 8: it is evident that the value of k_6 at $T = 340^\circ\text{C}$ is not aligned with the values calculated at the other temperatures, for this reason it was not used for the linear regression. This outcome is a further confirmation of the lower tendency to promote methanation reaction at lower temperature, in agreement with the evolution of the products distribution with contact times (Fig. 4) and the results of the model at 340°C (Fig. 7).

The calculated activation energies are:

$$E_{a,1} = 74 \text{ kJ/mol}$$

$$E_{a,2} = 104 \text{ kJ/mol}$$

$$E_{a,3} = 181 \text{ kJ/mol}$$

$$E_{a,4} = 47 \text{ kJ/mol}$$

$$E_{a,5} = 74 \text{ kJ/mol}$$

$$E_{a,6} = 8 \text{ kJ/mol}$$

These values are in agreement with literature [75–82].

3.4.4. Reaction pathway over Pt/Ni at 370°C

The results of the model have been also analyzed in terms of reactions rate vs. contact time, in order to study the contribution of each reaction, proceeding along the catalytic bed. The results at 370°C are very interesting: as shown in Fig. 9a, the first reactions are the ethanol dehydrogenation and decomposition, typically promoted at low temperature [45,70,71,73,75]. When contact times increase, hence proceeding along the catalytic bed, the subsequent reactions are the steam reforming of acetaldehyde and, with a less intense peak, its decomposition, in agreement with literature [71]. The water gas shift reaction has a considerable contribution, since it shows a higher peak compared to the steam reforming of acetaldehyde. The last reaction's step is the methanation reaction, with a peak of the relative reaction rate in the range 100–120 ms. At higher contact times, the experimental concentrations are close to the equilibrium values.

As a result of all these observations, besides the mathematical modelling of the reactions sequence at different temperature, it is possible to formulate a potential reaction pathway at 370°C for Pt/Ni, including different consecutive or parallel steps. It is schematically represented in Fig. 9b and described in the following lines: the ethanol could undergo a dissociative adsorption on the catalyst surface, as confirmed by literature [66–68] and observed by the results of TPD experiments (Fig. 9c). The signal of H_2 is

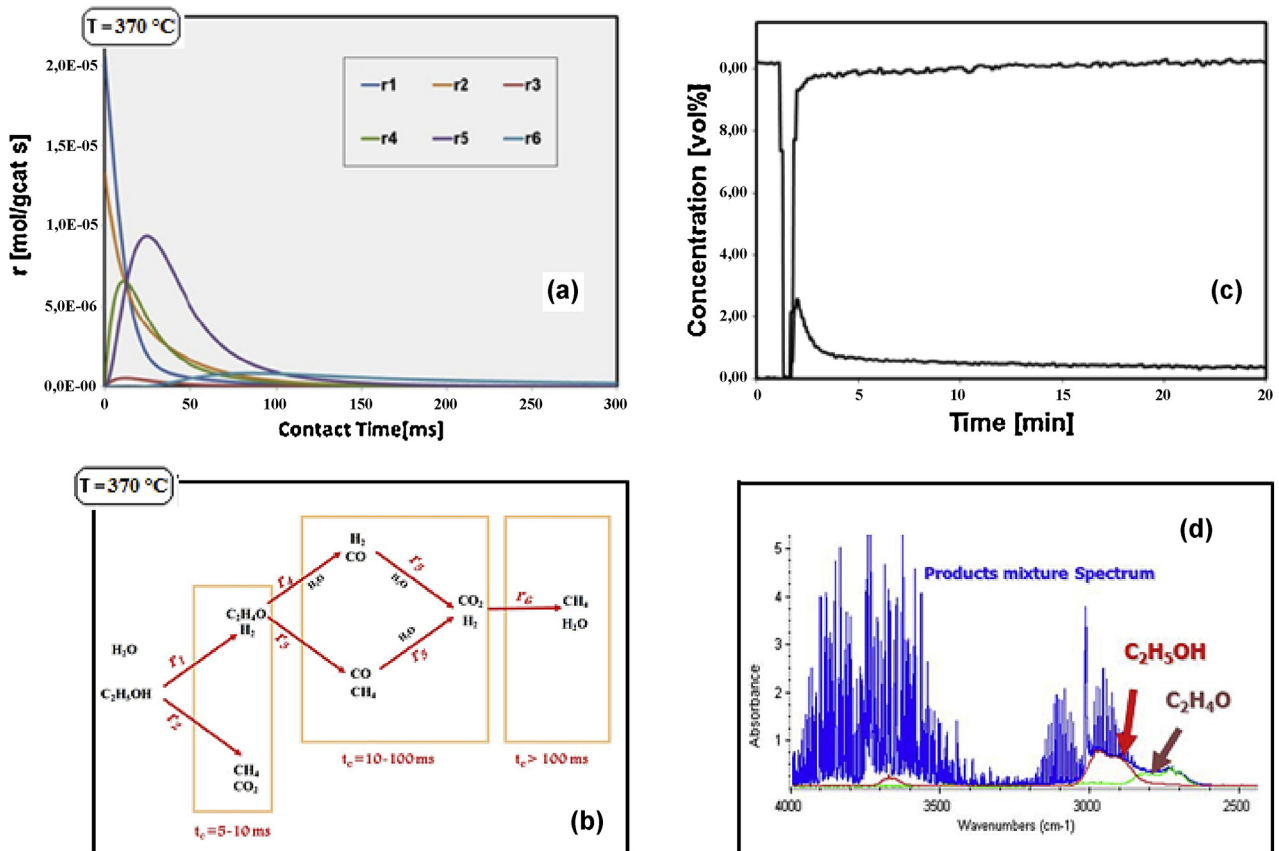


Fig. 9. Reaction sequence along the catalytic bed at 370 °C (a); reaction pathway at 370 °C (b); ethanol adsorption on Pt/Ni (c); FT-IR spectrum obtained during ethanol adsorption at $t = 3$ min (d).

inagreement with the tendency of ethanol, confirming the formation of an ethoxy species [83–86] and the formation of two atoms of hydrogen that form the molecule of H_2 . This justifies the assumption of the dehydrogenation of ethanol to acetaldehyde as the first reaction of the system [77,78,87], also considering that the acetaldehyde was detected in the FT-IR spectrum of the outlet gas stream (Fig. 9d).

It has been considered that the adsorbed ethanol could dehydrogenates to form an acetaldehyde intermediate [18,69]. Subsequently, the acetaldehyde may undergo a C–C bond rupture through two competitive reactions: decomposition to CO and CH_4 and steam reforming to CH_4 , CO and H_2 [61]. This is also established by analysing the evolution of the C-containing products during the desorption (here not reported): two peak for both CH_4 and CO , overlapped at 150 and 410 °C, were detected. The peaks at lower temperature can be related to the reactions of dehydrogenation of ethanol to acetaldehyde, followed by acetaldehyde decomposition and reforming. The second peak could be linked to additional decomposed acetaldehyde, in agreement with the results of the model and with literature, mainly producing CO and CH_4 [88]. The obtained carbon monoxide is converted into CO_2 and additional H_2 through the CO-WGS reaction. The last step is the methanation reaction, that enables the system to reach the equilibrium composition [18,34]. The hydrogen and water profiles were in agreement with the above hypothesis, thus validating the kinetic evaluation.

4. Conclusions

The performances of a bimetallic catalytic system, based on Pt (3 wt.%) and Ni (10 wt.%) and supported on CeO_2 , were investigated for the ethanol steam reforming at 250–600 °C.

The catalyst Pt/Ni revealed a good ability in the C–C bond rupture of the ethanol molecule, and this is ascribed to the well-known function of the nickel, enhanced by the platinum, that is directly available on the catalyst surface [79].

The sample showed high activity in the desired reaction, with a products distribution in agreement with the equilibrium calculation, yet at a low contact time (240 ms). The ethanol is completely converted, yet at $T > 300$ °C with high H_2 yield and a very low coke selectivity that allow the closure of the carbon mass balances in the range of the experimental error just by considering CH_4 , CO and CO_2 as C-containing products. The time-on-stream tests do not show deactivation, but were characterized by the reactor pressure drop increase, due to the carbon deposition, even if the coke selectivity and the coke formation rate are very low. Furthermore, it is not responsible for the deactivation of active sites and easily removed by using the real water-to-ethanol molar ratio in the feed stream instead of the stoichiometric one. As a conclusion, the sample is very interesting even for the activity and selectivity, and for the appreciable stability.

The evolution of the products distribution as a function of contact time (0–600 ms) and temperature (340–480 °C) was also examined with the purpose to model the reaction pathway. The set of reactions involved in the process was detected and it was proposed a possible reactions sequence at 370 °C including the following steps: ethanol adsorption followed by dehydrogenation to acetaldehyde; intermediate decomposition and reforming to CH_4 , CO , H_2 and CO_2 ; CO-WGS and CO_2 methanation reaction. The activation energy was also calculated for each reaction and the TPD experiments were used to validate the hypothesis on the reaction pathway.

Acknowledgments

This work has been partly funded by the European Commission through the FCH JU Project CoMETHy: Compact Multifuel-Energy To Hydrogen converter (GA No. 279075).

References

- [1] H.V. Fajardo, E. Longo, D.Z. Mezalira, G.B. Nuernberg, G.I. Almerindo, A. Colla-sioli, L.F.D. Probst, I.T.S. Garcia, N.L.V. Carren, *Environmental Chemical Letters* 8 (2010) 79–85.
- [2] V. Palma, A. Ricca, P. Ciambelli, *Clean Technologies and Environmental Policy* (March) (2012) 1–9, <http://dx.doi.org/10.1007/s10098-012-0477-2>.
- [3] P.N. Kechagiopoulos, S.S. Voutetakis, A.A. Lemonidou, I.A. Vasalos, *Catalysis Today* 127 (2007) 246–255.
- [4] E.C. Vagia, A.A. Lemonidou, *Applied Catalysis A-General* 351 (2008) 111–121.
- [5] F. Wang, W.C. Tana, H. Provendier, Y. Schuurman, C. Descorme, C. Mirodatos, W. Shena, *Applied Catalysis B: Environmental* 125 (2012) 546–555.
- [6] A. Haryanto, S.F.N. Murali, S. Adhikari, *Energy & Fuels* 19 (2005) 2098–2106.
- [7] M. Ni, D.Y.C. Leung, M.K.H.D. Leung, *International Journal of Hydrogen Energy* 32 (2007) 3238–3247.
- [8] M. Asif, T. Munir, *Renewable and Sustainable Energy Reviews* 11 (7) (2007) 1388–1413.
- [9] J.E. Mason, *Energy Policy* 35 (2) (2007) 1315–1329.
- [10] S. Freni, G. Maggio, S. Cavallaro, *Journal of Power Sources* 62 (1996) 67–73.
- [11] V. Palma, F. Castaldo, P.P. Ciambelli, G. Iaquinello, *Greenhouse Gases – Capturing Utilization and Reduction* 7 (2012) 137–184.
- [12] I. Fishtik, A. Alexander, R. Datta, D. Geana, *International Journal of Hydrogen Energy* 25 (2000) 31–45.
- [13] T. Ioannides, *Journal of Power Sources* 92 (2001) 17–25.
- [14] S. Cavallaro, V. Chiodo, S. Freni, N. Mondello, F. Frusteri, *Applied Catalysis A-General* 249 (2003) 119.
- [15] H. Roh, K. Jun, W. Dong, J. Chang, S. Park, Y. Joe, *Journal of Molecular Catalysis A: Chemical* 181 (2002) 137.
- [16] F. Haga, T. Nakajima, H. Miya, S. Mishima, *Catalysis Letters* 48 (1997) 223–227.
- [17] K. Vasudeva, N. Mitra, P. Umashankar, S.C. Dhingra, *International Journal of Hydrogen Energy* 21 (1996) 13–18.
- [18] L.-C. Chen, S.D. Lin, *Applied Catalysis B: Environmental* 106 (2011) 639–649.
- [19] A. Iulianelli, A. Basile, *International Journal of Hydrogen Energy* 35 (2010) 3170–3177.
- [20] V. Palma, E. Palo, F. Castaldo, P. Ciambelli, G. Iaquinello, *Chemical Engineering Transactions* 17 (2011) 947–952, <http://dx.doi.org/10.3303/CET1125158>.
- [21] F. Gallucci, F.A. Basile, S. Tosti, A. Iulianelli, E. Drioli, *International Journal of Hydrogen Energy* 32 (2007) 1201–1210.
- [22] A. Iulianelli, T. Longo, S. Liguori, P.K. Seelam, R.L. Keiski, A. Basile, *International Journal of Hydrogen Energy* 34 (2009) 8558–8565.
- [23] A. Iulianelli, S. Liguori, T. Longo, S. Tosti, P. Pinacci, A. Basile, *International Journal of Hydrogen Energy* 35 (2010) 3159–3164.
- [24] P.K. Seelam, S. Liguori, A. Iulianelli, P. Pinacci, V. Calabro, M. Huuhutanen, R. Keiski, V. Piemonte, S. Tosti, M. De Falco, A. Basile, *Catalysis Today* 193 (2012) 42–48.
- [25] V. Palma, F. Castaldo, P. Ciambelli, G. Iaquinello, *Chemical Engineering Transactions* 29 (2012) 109–114, <http://dx.doi.org/10.3303/CET1229019>.
- [26] P. Ciambelli, V. Palma, A. Ruggiero, *Applied Catalysis B: Environmental* 96 (2010) 18–27.
- [27] P. Ciambelli, V. Palma, A. Ruggiero, *Applied Catalysis B: Environmental* 96 (2010) 190–197.
- [28] T. Yamazaki, N. Kikuchi, M. Katoh, T. Hirose, H. Saito, T. Yoshikawa, M. Wada, *Applied Catalysis B: Environmental* 99 (2010) 81–88.
- [29] M.S. Batista, R.K.S. Santos, E.M. Assaf, J.M. Assaf, E.A. Ticianelli, *Journal of Power Sources* 134 (2004) 27–32.
- [30] A. Denis, W. Grzegorczyk, W. Gac, A. Machocki, *Catalysis Today* 137 (2008) 453–459.
- [31] C. Rioche, S. Kulkarni, F.C. Meunier, J.P. Breen, R. Burch, *Applied Catalysis B: Environmental* 61 (2005) 130–139.
- [32] F. Aupretre, C. Descorme, D. Duprez, *Catalysis Communications* 3 (2002) 263.
- [33] H.S. Roh, A. Platon, Y. Wang, D.L. King, *Catalysis Letters* 110 (2006) 1–2, <http://dx.doi.org/10.1007/s10562-006-0082-2>.
- [34] J.P. Breen, R. Burch, H.M. Coleman, *Applied Catalysis B: Environmental* 39 (2002) 65.
- [35] A.E. Galetti, M.F. Gomez, L.A. Arrua, M.C. Abello, *Applied Catalysis A-General* 408 (2011) 78–86.
- [36] J.J. Carroll, K.L. Haug, J.C. Weisshaar, M.R.A. Blomberg, P.E.M. Siegbahn, M. Svensson, *The Journal of Physical Chemistry* 99 (1995) 13955–13969.
- [37] C. Diagne, H. Idriss, A. Kiennemann, *Catalysis Communications* 3 (2002) 565–571.
- [38] F. Aupretre, C. Descorme, D. Duprez, *Topics in Catalysis* 30/31 (2004) 487–491.
- [39] P.-Y. Sheng, A. Yee, G.A. Bowmaker, H. Idriss, *Journal of Catalysis* 208 (2002) 393–403, <http://dx.doi.org/10.1006/jcat.2002.3576>.
- [40] A. Le Valant, A. Garron, N. Bion, F. Epron, D. Duprez, *Catalysis Today* 138 (2008) 169–174.
- [41] P. Djinovic, J. Batista, B. Cehic, A. Pintar, *Journal of Physical Chemistry A* 114 (2010) 3939–3949.
- [42] A. Erdohelyi, J. Raskó, T. Kecskés, M. Tóth, M. Dömök, K. Baán, *Catalysis Today* 116 (2006) 367–376.
- [43] M. Akiyama, Y. Oki, M. Nagai, *Catalysis Today* 181 (2012) 4–13.
- [44] J. Llorca, N. Homs, J. Sales, R.P. de la Piscina, *Journal of Catalysis* 209 (2002) 306–317.
- [45] H. Idriss, C. Diagne, J.P. Hindermann, A. Kiennemann, M.A. Barteau, *Journal of Catalysis* 155 (1995) 219–237.
- [46] F. Marino, E.G. Cerrella, S. Duhalde, M. Jobbagy, M.A. Laborde, *International Journal of Hydrogen Energy* 23 (1998) 1095.
- [47] F. Marino, M. Boveri, G. Baronetti, M. Laborde, *International Journal of Hydrogen Energy* 26 (2001) 665.
- [48] F. Marino, G. Baronetti, M. Jobbagy, M. Laborde, *Applied Catalysis A-General* 6043 (2002) 1.
- [49] A. Fatsikostas, D. Kondarides, X. Verykios, *Catalysis Today* 75 (2002) 145.
- [50] D. Liguras, D. Kondarides, X. Verykios, *Applied Catalysis B: Environmental* 43 (2003) 345.
- [51] A. Ruggiero, PhD thesis, University of Salerno, 2009.
- [52] B. Wang, A.K. Gupta, J. Huang, H. Vedala, Q. Hao, V.H. Crespi, W. Choi, P.C. Eklund, *Physical Review B* 81 (2010) 115422.
- [53] S.S.-Y. Lin, H. Daimon, S.Y. Ha, *Applied Catalysis A-General* 366 (2009) 252–261.
- [54] E. Heracleous, A.F. Leeb, K. Wilson, A.A. Lemonidou, *Journal of Catalysis* 231 (2005) 159–171.
- [55] H. Song, U.S. Ozkan, *Journal of Catalysis* 261 (2009) 66–74.
- [56] R.W. McCabe, C. Wong, H.S. Woo, *Journal of Catalysis* 144 (1988) 354–367.
- [57] T. Parryczak, J. Rynkowski, S. Karski, *Journal of Chromatography A* 188 (1980) 254–256.
- [58] H. Chen, H. Yu, F. Peng, H. Wang, J. Yang, M. Pan, *Journal of Catalysis* 269 (2010) 281–290.
- [59] E. Akpan, A. Akande, A. Aboudheir, H. Ibrahim, R. Idem, *Chemical Engineering Science* 62 (2007) 3112–3126.
- [60] M. Araque, J.C. Vargas, *International Journal of Hydrogen Energy* 36 (2011) 1491–1502.
- [61] M.N. Barroso, M.F. Gomez, *Chemical Engineering Journal* 158 (2010) 225–232.
- [62] M.S. Batista, R.K.S. Santos, *Journal of Power Sources* 124 (2003) 99–103.
- [63] A. Kazama, Y. Sekine, *Applied Catalysis A-General* 383 (2010) 96–101.
- [64] A.F. Lucedio, J.D.A. Bellido, *Fuel* 90 (2011) 1424–1430.
- [65] R. Padilla, M. Benito, *International journal of hydrogen energy* 35 (2010) 8921–8928.
- [66] C. Wu, P.T. Williams, *Applied Catalysis B: Environmental* 102 (2011) 251–259.
- [67] A. Carrero, J.A. Calles, *Applied Catalysis A-General* 327 (2007) 82–94.
- [68] M. Lindo, A.J. Vizcaino, *International Journal of Hydrogen Energy* 35 (2010) 5895–5901.
- [69] A.M. da Silva, L.O.O. da Costa, *Catalysis Communications* 11 (2010) 736–740.
- [70] A. Casanovas, J. Llorca, *Journal of Molecular Catalysis A: Chemical* 250 (2006) 44–49.
- [71] S. Cavallaro, *Energy & Fuels* 14 (2000) 1195–1199.
- [72] F. Frusteri, S. Freni, *Applied Catalysis A-General* 270 (2004) 1–7.
- [73] S.S. Freni, S. Cavallaro, *Catalysis Communications* 4 (2003) 259–268.
- [74] J.J. Llorca, R.P. de la Piscina, *Applied Catalysis B: Environmental* 43 (2003) 355–369.
- [75] S.M. de Lima, A.M. da Silva, *Applied Catalysis B: Environmental* 96 (2010) 387–398.
- [76] W.F. Podolski, G.K. Young, *Industrial & Engineering Chemistry Process Design and Development* 13 (1974) 415–442.
- [77] A.P. Farkas, F. Solymosi, *Surface Science* 601 (2007) 193–200.
- [78] H. Song, U.S. Ozkan, *Catalysis Letters* 141 (2011) 43–54.
- [79] M.C. Sanchez-Sanchez, R. Navarro Yerga, *Journal of Physical Chemistry A* 114 (2010) 3873–3882.
- [80] R.J. Byron Smith, M. Loganathan, S. Murthy Shekhar, *International Journal of Chemical Reaction Engineering* 8 (2010).
- [81] R. Barthos, A. Széchenyi, A. Koos, F. Solymosi, *Applied Catalysis A-General* 327 (2007) 95–105.
- [82] A. Gazisib, A. Koos, T. Bansagi, F. Solymosi, *Catalysis Today* (2011), 160.
- [83] D. Sannino, V. Vaiano, P. Ciambelli, *Catalysis Today* (2012), <http://dx.doi.org/10.1016/j.cattod.2012.07.038>
- [84] D. Sannino, V. Vaiano, P. Ciambelli, M.C. Hidalgo, J.J. Murcia, J.A. Navío, *Journal of Advanced Oxidation Technologies* 15 (2) (2012) 284–293.
- [85] J.J. Murcia, M.C. Hidalgo, J.A. Navío, V. Vaiano, P. Ciambelli, D. Sannino, *Catalysis Today* 196 (2012) 101–109.
- [86] J.J. Murcia, M.C. Hidalgo, J.A. Navío, V. Vaiano, P. Ciambelli, D. Sannino, *International Journal of Photoenergy* 2012 (2012), Article ID 687262, 9 pages, <http://dx.doi.org/10.1155/2012/687262>
- [87] A.N. Fatsikostas, X.E. Verykios, *Journal of Catalysis* 225 (2004) 439–452.
- [88] S.M. de Lima, A.M. da Silva, *Journal of Catalysis* 268 (2009) 268–281.